Supplementary Information

Development of sustained anticancer drug delivery system based on hybridization between diatomite and nanostructured lipid carriers

Sunggu Kang[a,†], Daehyeon Yoo[a,†], Yoseph Seo[a,†], Daeryul Kwon[b], Yeeun Woo[a], Hyeok Ki Kwon[a], Jungbum Kim[c], Jinyoung Park[c], Wonhwa Lee[c,d], Suk Min Yun[e], Sang Deuk Lee[f], and Taek Lee[a,*]

[a] *Department of Chemical Engineering, Kwangwoon University, 20 Kwangwoon-ro, Nowon-gu, Seoul 01897, Republic of Korea*

[b] *Biological Resources Assessment Division, National Institute of Biological Resourses, Hwangyeong-ro 42, Seo-gu, Incheon, 22689, Korea*

[c] *Department of Chemistry, College of Science, Sungkyunkwan University, 2066 Seobu-ro, Jangan-gu, Suwon 16419, South Korea*

[d] *Department of MetaBioHealth, Institute for ICS, Sungkyunkwan University, Suwon, 16419, Republic of Korea*

[e] *Biological Resources Research Department, Nakdonggang National Institute of Biological Resources, Sangju-si, Gyeongsangbuk-do 37242, Republic of Korea*

[f] *Protist Research Division, Biological Resources Research Department, Nakdonggang National Institute of Biological Resources (NNIBR), 137, Donam 2-gil, Sangju-si 37242, Gyeongsangbuk-do, Republic of Korea*

*Address correspondence to: tlee@kw.ac.kr (T.L.)

†These authors contributed equally to this work.

Table of contents

1. Synthesis of the amphiphilic chitosan

1.1. Synthesis of amphiphilic acylated chitosan

Acylated chitosan was synthesized using a previously established method[1], starting with low molecular weight chitosan (MW = 12,000 g/mol). Lauryl aldehyde was added to chitosan at a molar ratio of 1:0.3 and stirred for over 12 h to facilitate the reaction. Subsequently, sodium borohydride ($NaBH_4$) was introduced at a molar ratio of 1:3 (relative to chitosan) under acidic conditions (pH 5) and stirred for an additional 3 h to complete the reduction process. The reaction solution was then neutralized (pH 7), causing the precipitation of hydrophilic chitosan, which was collected through filtration and washed sequentially with ethanol (from 70% to 100%). Finally, the purified chitosan was freeze-dried to yield the alkylated product in powder form.

1.2. Characterization of amphiphilic acylated chitosan

The degree of substitution was determined using proton nuclear magnetic resonance (^{1}H NMR) spectroscopy. For this analysis, samples were prepared by dissolving 5 mg/mL of the polymer in 0.2 M CD_3COOD. The ^{1}H NMR spectra were recorded at 80°C using a Varian Unity Plus 300 spectrometer (Garden State Scientific, Morristown, NJ, USA). The calculation of the degree of substitution was based on the digital integration of the CH_3 protons from the acyl chain and the anomeric proton of chitosan, as illustrated in Figure S1 (A), (B). The degree of substitution was determined to be 8.58% by Equation S1 as followed:

$$Substitution\ Degree\ (\%) = 100 \times \frac{I(H7)/3}{I(H1)} \qquad \text{(Equation S1)}$$

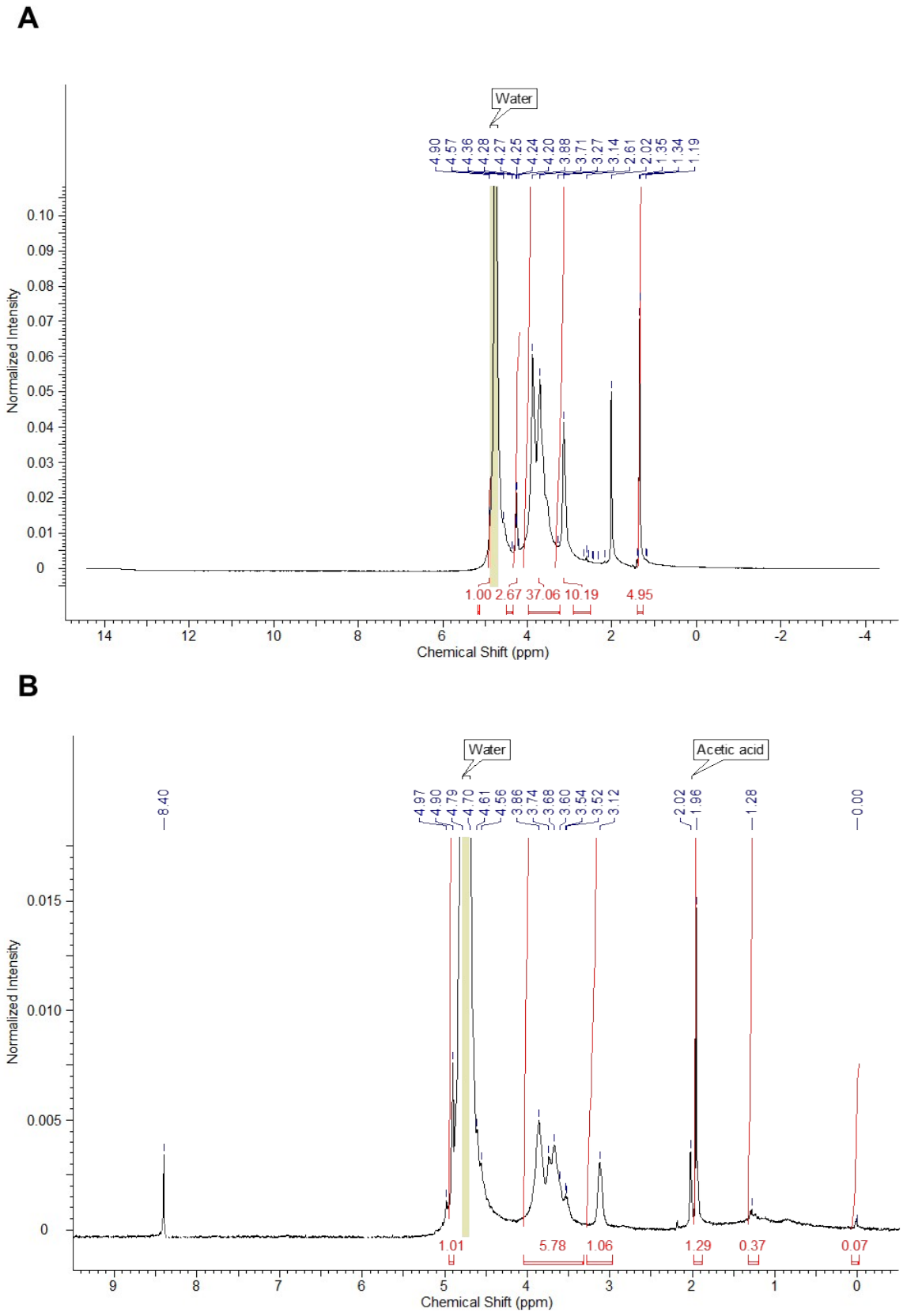

Figure S1. (A) NMR spectrum of non-acylated chitosan. (B) NMR spectrum of acylated chitosan.

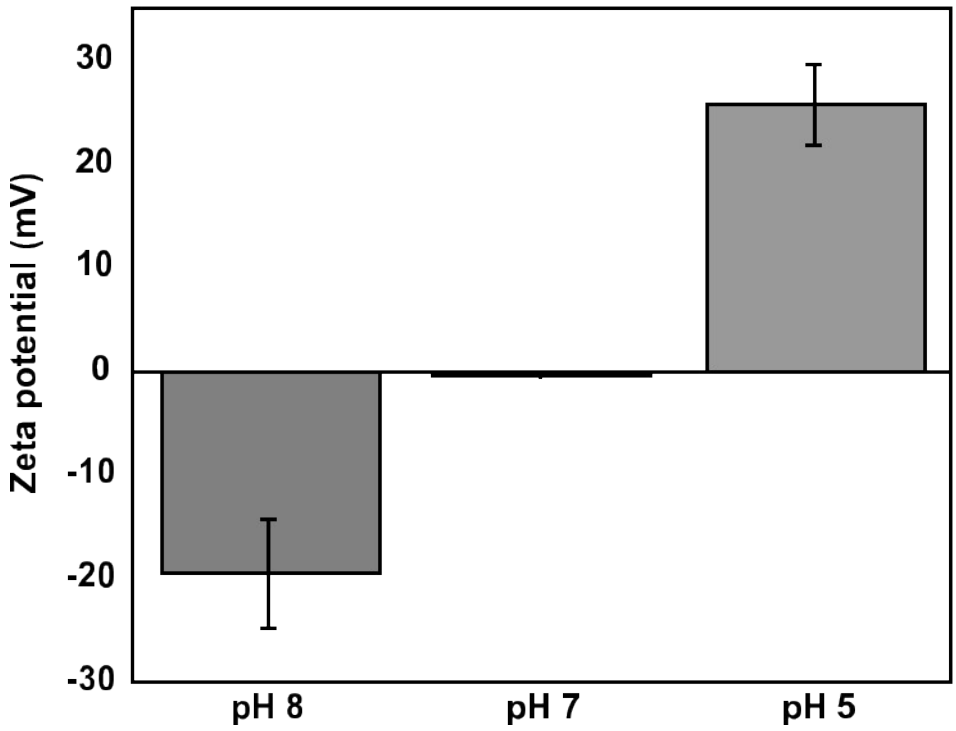

Figure S2. Zeta potential of DB under various pH conditions.

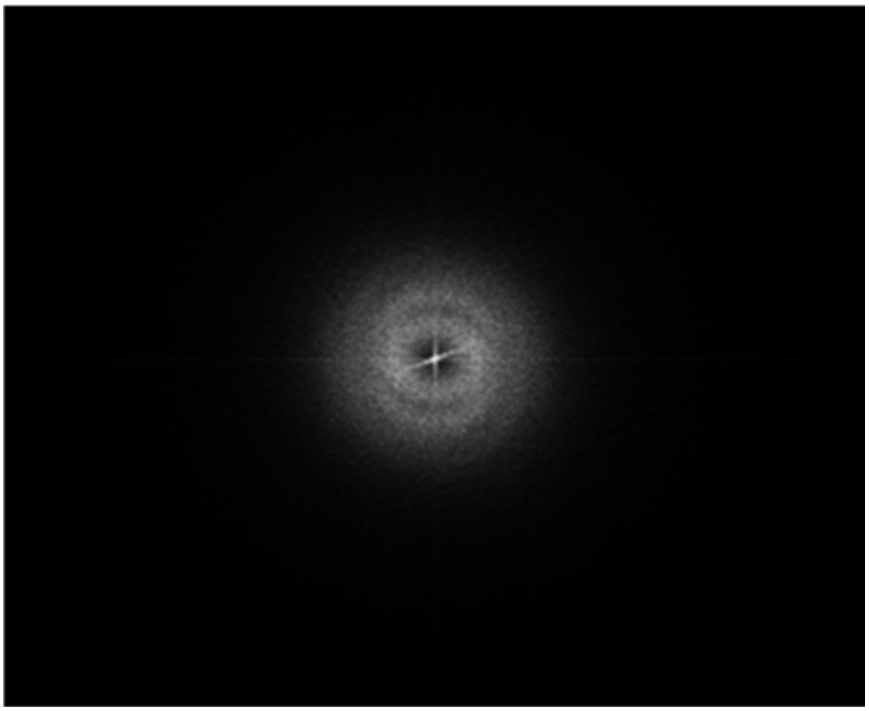

Figure S3. FFT analysis of the diffraction pattern to verify the amorphous structure of DB.

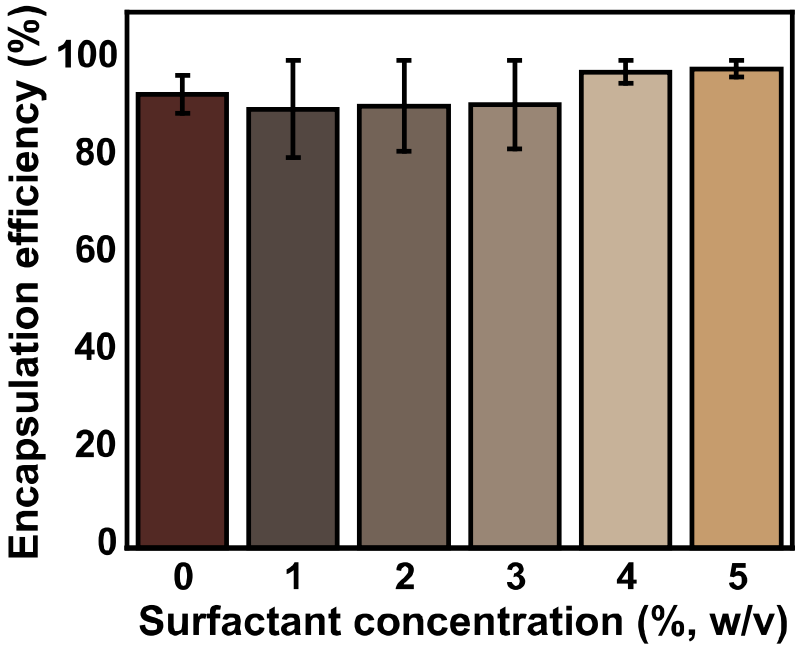

	Drug encapsulation efficiency (%)	Loading capacity (%)
cNLC 12	98.27 ± 1.73 %	4.65 ± 0.15 %

Figure S4. Drug encapsulation efficiency (%) and loading capacity (%) of DOX-cNLC under various surfactant concentrations.

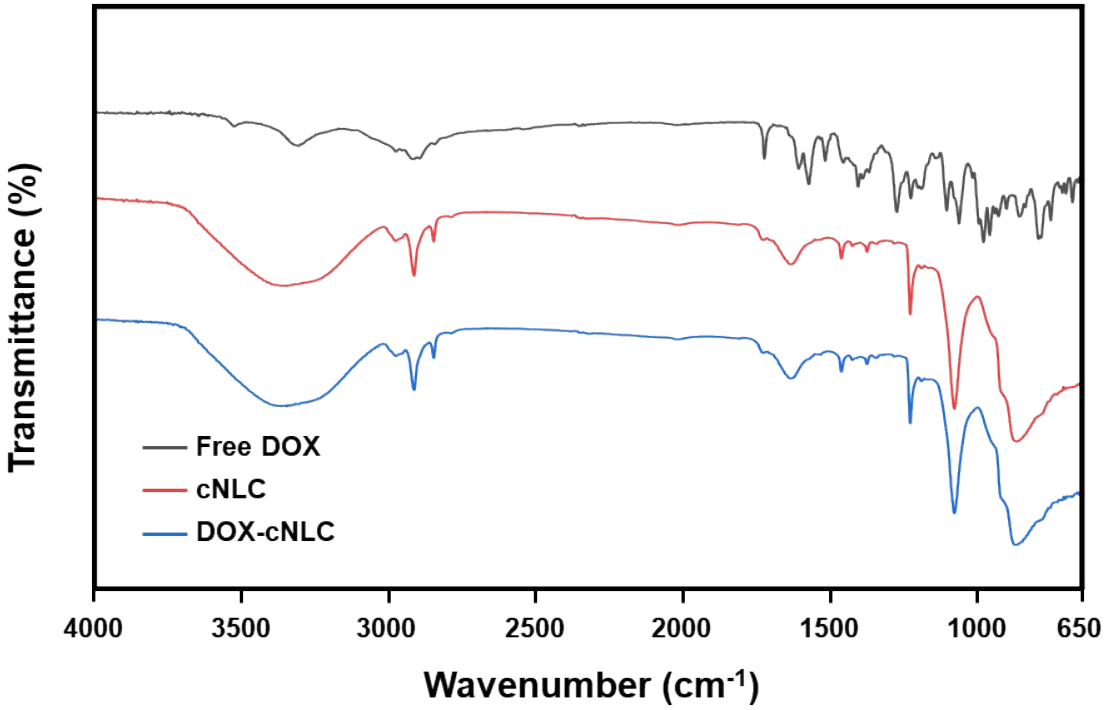

Figure S5. FT-IR spectra of free DOX, cNLC, and DOX-cNLC showing characteristic functional groups and interactions.

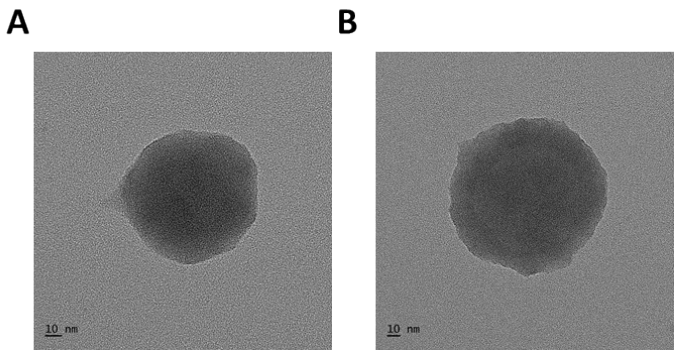

Figure S6. TEM analysis results of (A) cNLC and (B) DOX-cNLC morphology.

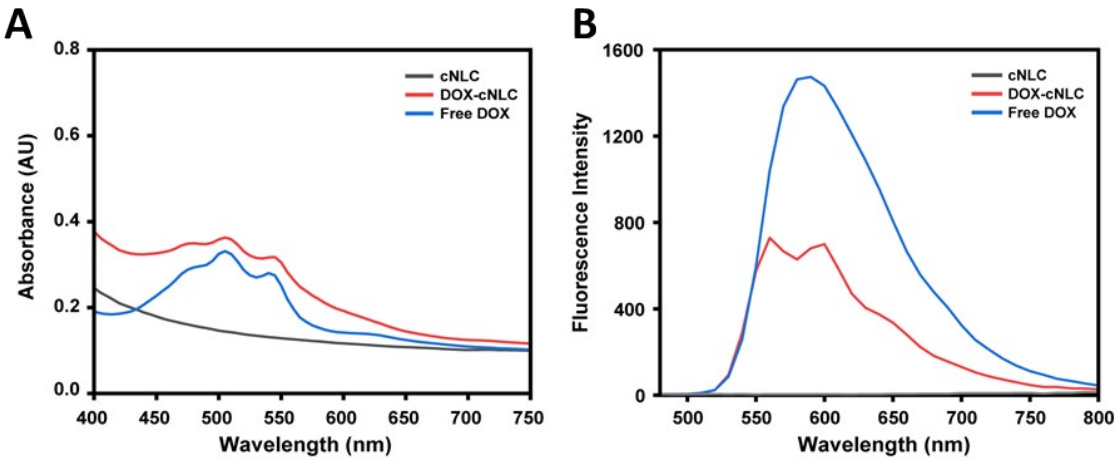

Figure S7. (A) UV–Vis absorption spectra and (B) Fluorescence emission spectra of blank cNLC, DOX-cNLC, and free DOX.

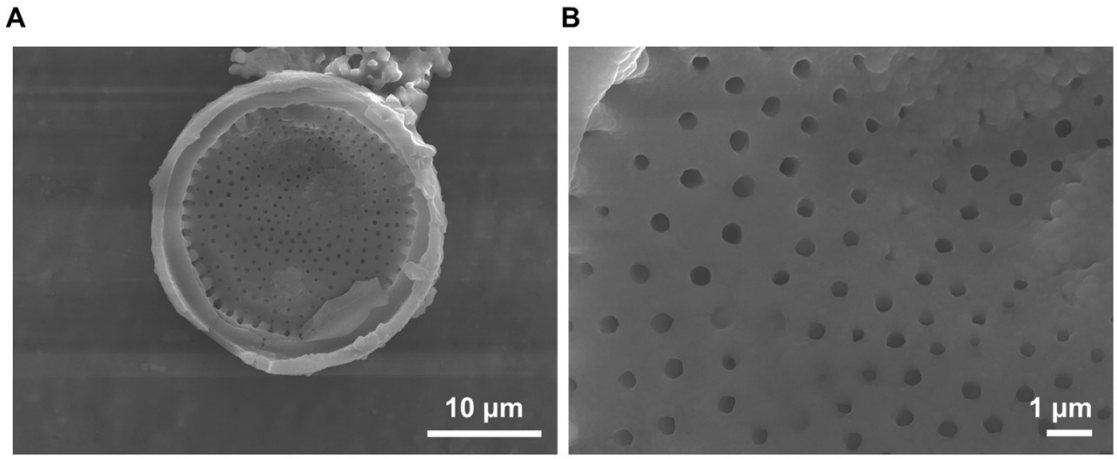

Figure S8. SEM analysis results of (A) DBNC and (B) the enlarged SEM image of (A), highlighting the preserved porous structure of DB with clearly visible pore entrances following cNLC loading.

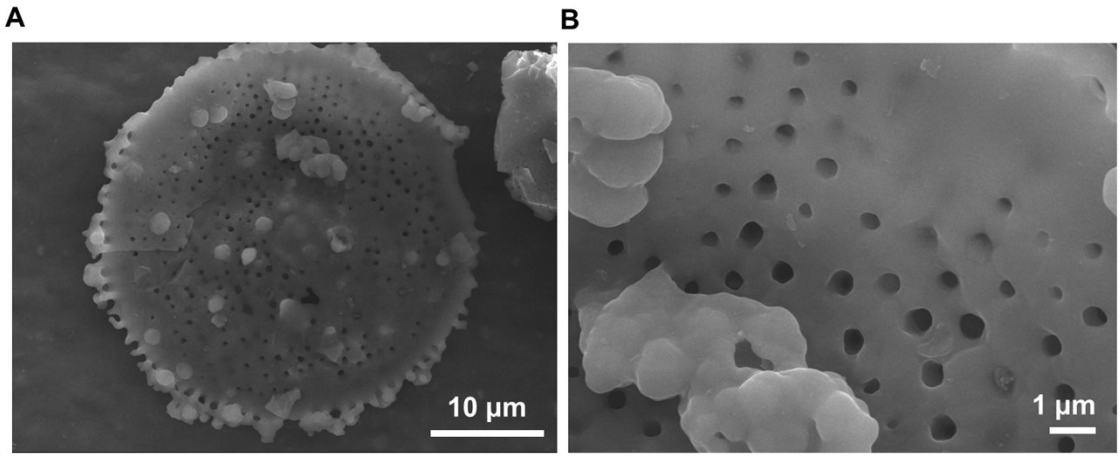

Figure S9. (A) SEM image of the DOX-DBNC. (B) Enlarged SEM image of DOX-DBNC.

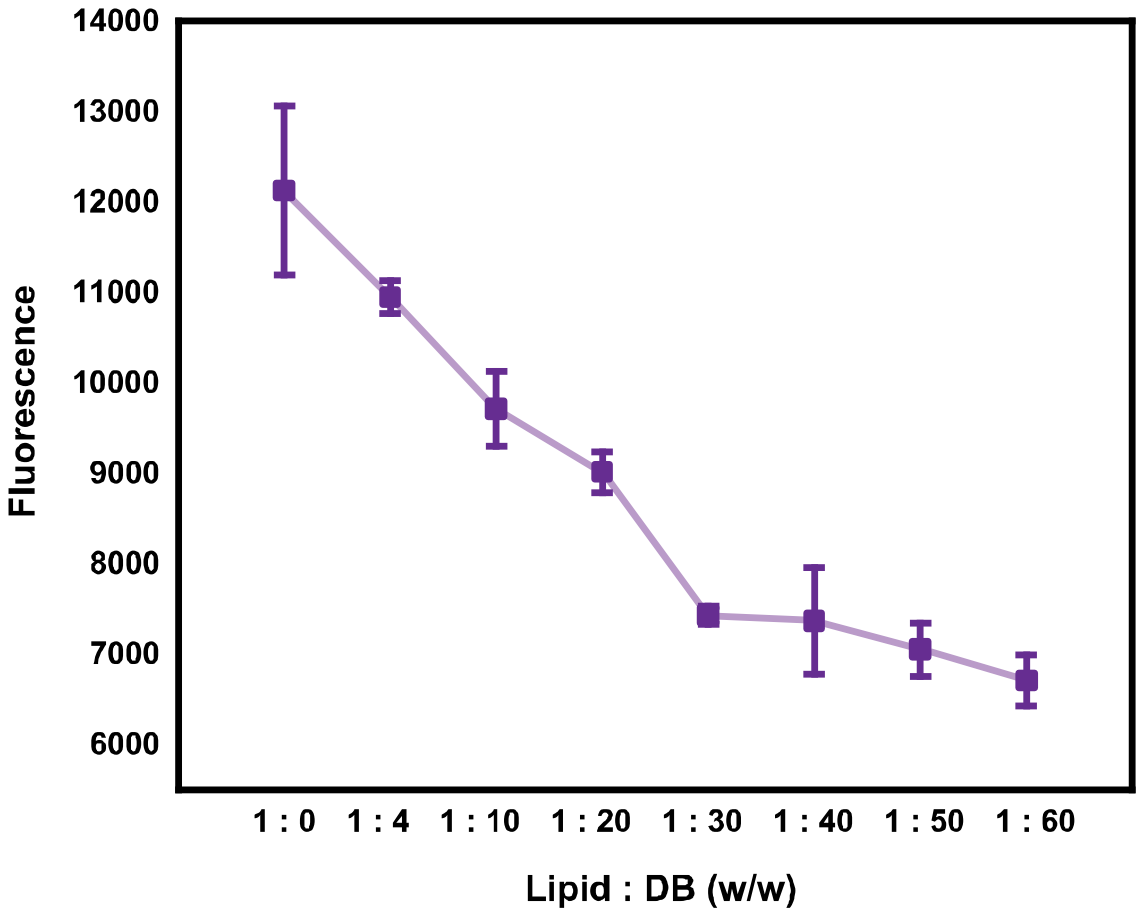

Figure S10. Optimization results of the adhesion ratio of DB and cNLC (w/w %) through fluorescence analysis

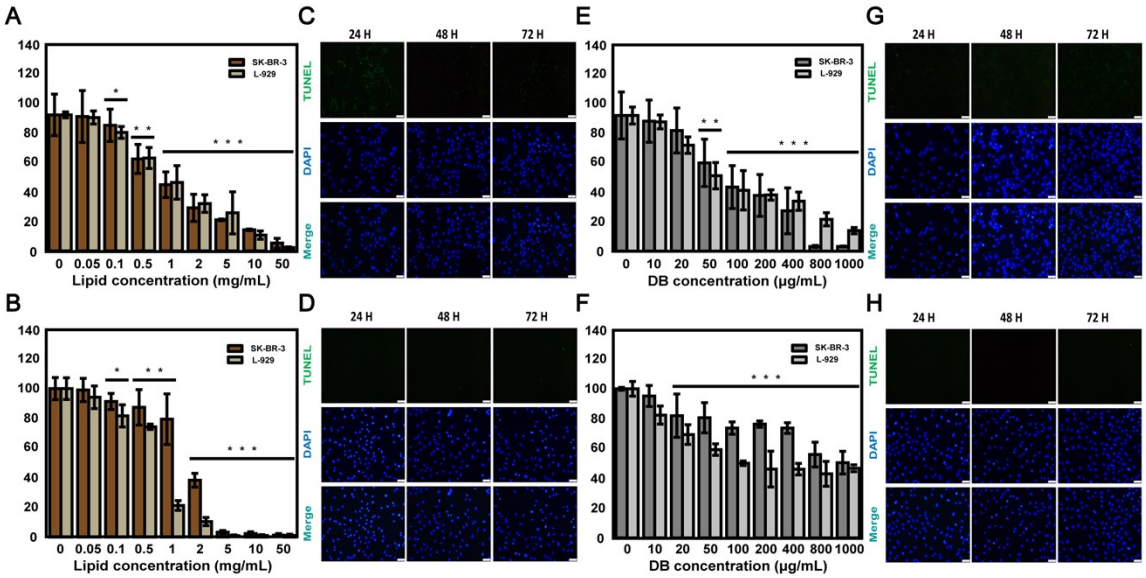

Figure S11. (A) Cytotoxicity evaluation of cNLC at varying concentrations (after 24 h). (B) Cytotoxicity evaluation of cNLC at varying concentrations (after 72 h). (C) Time-dependent apoptosis evaluation via TUNEL staining in SK-BR-3 cells treated with cNLC. (D) Time-dependent apoptosis evaluation via TUNEL staining in L-929 cells treated with cNLC. (E) Cytotoxicity evaluation of DB at varying concentrations (after 24 h). (F) Cytotoxicity evaluation of DB at varying concentrations (after 72 h). (G) Time-dependent apoptosis evaluation via TUNEL staining in SK-BR-3 cells treated with DB. (H) Time-dependent apoptosis evaluation via TUNEL staining in L-929 cells treated with DB. Scale bars represent 50 μm. Statistical analysis of cell viability was conducted in comparison to the control group (Concentration 0 μM), with significance levels indicated as *p<0.05, **p<0.01, and ***p<0.001.

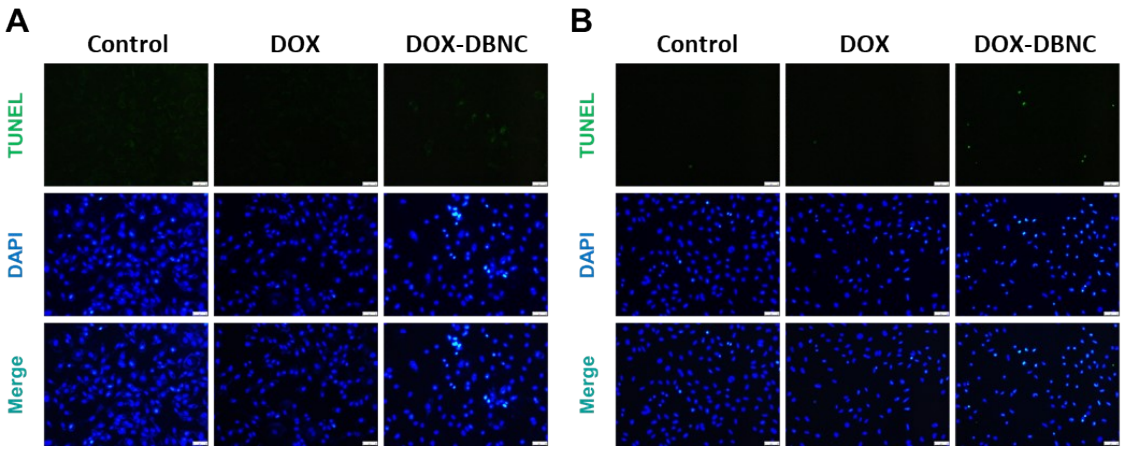

Figure S12. Apoptosis evaluation via TUNEL staining in (A) SK-BR-3 and (B) L-929 cells 48 h after drug administration. Scale bars represent 50 μm.

Table S1. Particle size, polydispersity index and ζ potential of lipid nanoparticles with varying amounts of surfactant (% w/v).

No.	Tween 80 (%)	Poloxamer 407 (%)	D_{18}DAB (%)	Lipid (%)	Particle size (nm)	Polydispersity Index (PDI)	Zeta potential (mV)
Surfactant-free cNLC	0	0	0.5	4.5	9087.2 ± 614.4	2.2 ± 0.2	-
cNLC 1	0.5	0.5	0.5	4.5	381.47 ± 46.14	0.268 ± 0.013	25.88 ± 0.46
cNLC 2	1.0	0.5	0.5	4.5	146.45 ± 0.78	0.228 ± 0.010	27.21 ± 1.55
cNLC 3	0.5	1.0	0.5	4.5	149.07 ± 2.15	0.233 ± 0.014	25.67 ± 0.66
cNLC 4	1.5	0.5	0.5	4.5	115.00 ± 2.08	0.252 ± 0.009	27.81 ± 2.90
cNLC 5	1.0	1.0	0.5	4.5	123.43 ± 0.75	0.236 ± 0.006	25.09 ± 1.79
cNLC 6	0.5	1.5	0.5	4.5	129.73 ± 1.00	0.184 ± 0.009	26.76 ± 1.40
cNLC 7	2.0	0.5	0.5	4.5	105.67 ± 0.68	0.196 ± 0.017	26.98 ± 0.83
cNLC 8	1.5	1.0	0.5	4.5	101.90 ± 1.51	0.184 ± 0.010	28.55 ± 0.19
cNLC 9	1.0	1.5	0.5	4.5	110.47 ± 0.29	0.192 ± 0.018	26.79 ± 1.57
cNLC 10	0.5	2.0	0.5	4.5	120.9 ± 0.72	0.243 ± 0.005	25.69 ± 1.43

cNLC 11	2.5	0.5	0.5	4.5	71.10 ± 1.25	0.208 ± 0.007	27.49 ± 0.20
cNLC 12	2.0	1.0	0.5	4.5	84.53 ± 2.40	0.211 ± 0.007	29.35 ± 1.42
cNLC 13	1.5	1.5	0.5	4.5	77.47 ± 0.76	0.205 ± 0.013	29.22 ± 1.18
cNLC 14	1.0	2.0	0.5	4.5	82.83 ± 0.47	0.211 ± 0.007	25.50 ± 0.23
cNLC 15	0.5	2.5	0.5	4.5	83.97 ± 5.62	0.22 ± 0.012	28.37 ± 4.37

Table S2. ΔH_{app} value extracted from ITC analysis under low (20 mM) and high (300 mM) ionic strength conditions. Initial injections (1^{st}) and averaged injections (1 to 8) were analyzed to compare salt-dependent changes in heat release.

Buffer condition (mM)	Q of first injection (µJ)	ΔH_{app} of first injection (kJ/mol)	Average Q of 1 to 8 injections (µJ)	Average ΔH_{app} of 1 to 8 injections (kJ/mol)
20	- 126.8	- 101.4	- 103.7 ± 24.9	- 82.9 ± 19.9
300	8.2	6.6	2.6 ± 8.4	2.1 ± 6.7

Supplementary References

1 Ö. Tezgel, A. Szarpak-Jankowska, A. Arnould, R. Auzély-Velty and I. Texier, *J. Colloid Interface Sci.*, 2018, **510**, 45–56.